Design comparison of surface-mounted permanent magnet synchronous motors with inner and outer rotor configurations

Hoang Bui Huu[1], Bao Doan Thanh[2], Tran Duc Chuyen[3], Vuong Dang Quoc[1]
[1]School of Electrical and Electronic Engineering, Hanoi University of Science and Technology, Hanoi, Vietnam
[2]Faculty of Engineering and Technology, University of Quy Nhon, Quy Nhon, Vietnam
[3]Faculty of Electrical Engineering-Automation, University of Economics - Technology for Industries, Hanoi, Vietnam

Article Info

Article history:

Received Mar 10, 2024
Revised Aug 13, 2024
Accepted Aug 29, 2024

Keywords:

Analytical model
EMF
Finite element analysis
IPMSM
SPMSM
Torque ripple

ABSTRACT

The surface-mounted permanent magnet synchronous motor (SPMSM) is one of the electric machines applied widely in the fields of electric vehicles (EVs) and electrical drives due to their good characteristics such as high power density, lower mass, high efficiency, and lower torque. For the SPMSM, there are two types of SPMSM, i.e., the inner rotor SPMSM and the outer rotor SPMSM. To analyze and compute advantages and disadvantages, as well as to compare the performances of these two motor types, this research proposes an analytical model to design preliminarily the main/required parameters of the SPMSM with inner and outer rotor types. Subsequently, a finite element method is developed to simulate, analyze, and compare the electromagnetic parameters of the proposed motors. Via the developed methods, the obtained results will also indicate the performances of both types of motors. In particular, it will provide a good recommendation for choosing the SPMSM with an inner or outer rotor structure for traction applications.

Corresponding Author:

Vuong Dang Quoc
School of Electrical and Electronic Engineering, Hanoi University of Science and Technology
Dai Co Viet Street, Hai Ba Trung District, Hanoi City, Viet Nam
Email: vuong.dangquoc@hust.edu.vn

1. INTRODUCTION

Surface-mounted permanent magnet synchronous motors (SPMSMs) are becoming more and more common in electrical drives and electric vehicles (EVs) as a result of industrialization and technological advancements [1], [2]. The permanent magnet (PM) for the SPMSM is fixed straight onto the rotor surface. This integration contributes to lower energy consumption and increases torque, economy, and stability. Additionally, this machine finds application in industrial domains such as motion control and compressors [3]. Aside from that, it can also be utilized in mining, oil extraction, lifting and lowering systems, electric drive systems, marine propulsion, and high-torque low-speed applications, especially in the context of rare-earth magnet development [4].

The SPMSM is divided into two types of motors: inner rotor SPMSM and outer rotor SPMSM, depending on the rotor position. Each of these two motors has benefits and drawbacks of its own. Based on strong arguments, the study in reference [5] suggested that a permanent magnet synchronous motor (PMSM) with an outside rotor be preferred. To prove that, two different methods were used. The first method compares two possible PM motor topologies' torque capacities by examining their individual geometrical volumes. The second compares the PM motor to a magnetic circuit topology that is the same, but in this case, the rotor can be thought of as both an inner and an outer rotor. The PM flux density of inner and outer rotor SPMSMs used in electric bicycle applications was calculated and compared using a finite element method (FEM) in [6]. However, this contribution did not offer the process of designing this motor; rather, it only focused on simulation to obtain the results.

Several coaxial magnetic gear designs were presented in reference [7] for flux modulators to examine and contrast torque characteristics. Using a 2-D finite element analysis, the torque properties of the proposed shapes were determined through the nonlinear model. The study also constructed a design with slot and pole combinations for the interior PMSM (IPMSM) and SPMSM, as references [8]-[10] show. Total harmonic distortions (THDs), cogging torque, back electromotive force (EMF), torque ripple, and loss characteristics were all compared in these experiments using an analytical model. The FEM in reference [11] produced an optimal design of the IPMSM utilized in electric and hybrid vehicles to ascertain the ideal current levels for both the efficiency and the cogging torque. The data also showed how the cogging torque affected the motor's noise and vibration. The study examined the effects of various design factors on the cogging torque produced by PM machines in reference [12]. It was also taken into consideration how significantly the slot and pole combinations affected the cogging torque. The comprehensive performance of multi-physics for the surface-mounted permanent magnet or SPM and interior permanent magnet or IPM was compared and examined in references [13], [14]. The 60 kW and 30.000 rpm initial circumstances for the development of the SPM and IPM designs kept the same stator architectures, winding types, and volumes. Then, using Ansys Workbench, a FEM was built to guarantee that the stress-field requirements for both rotor structures were followed. Analysis of the effects of different parameters on rotor stress was done methodically. Individual models for the IPMSM with multiple-layer PMs were developed in reference [15] to preserve the same stator structure, winding type, and PM volume. The FEM was also suggested as a way to compare the electromagnetic characteristics, such as inductance, torque, and efficiency, of the SPMSM and IPMSM kinds.

The results showed that employing the double-layer PMs enhanced the conspicuous features. The research in reference [16] also looked into how well-suited SPM and IPM motors are for high-speed applications. These two motors have the same power/speed ratios and important parameters thanks to their careful design. Specifically, the electromagnetic parameters and demagnetization characteristics of the IPMSM and SPMSM were evaluated and assessed using the FEM in this research. Then, a lumped parameter thermal network was employed to assess each of their individual thermal performances. According to the simulated results, the IPM motor has better torque per PM weight and comparable electromagnetic performance to the SPM motor in high-speed operations. However, it was also observed that the IPM motor's rotor construction is less durable and more prone to irreversible demagnetization. A study comparing four distinct rotor configurations used in a high-speed PMSM was published in reference [17]. To evaluate and assess the rotor stresses under different influencing conditions, a 3D FEM was used. In particular, the study looked at how interference, sleeve thickness, and temperature rise affected the stresses in various rotor structures. The strains placed on these rotor constructions were then examined in a variety of operating scenarios.

As analyzed above, so far, many articles have worked on SPM and IPM motors, as well as a comparison of their performances. However, these studies primarily concentrate on simulating the SPM or IPM motor by using the FEM or experimental model to give results. These studies have not yet presented the detail of the analytical process for computing electromagnetic parameters, and also for comparing the performances of these motors. In this research, the new contribution is that the analytical model is developed in detail to define the required parameters of the SPMS with inner and outer rotor configurations. And then, the FEM is approached to simulate and compare the performances of these machines, such as the flux density, output torque, cogging torque, back electromagnetic force (EMF), flux linkage, and temperature rise. The obtained results will be considered as a valuable reference for choosing the SPMSM with inner or outer rotor structure for traction applications.

In section 2, the analytical design of the inner and outer rotor SPMSMs is presented to show the detail of a design process for two different rotor configurations. In section 3, a 3D-FEM is conducted for different rotor structures to calculate and compare the electromagnetic parameters of two of these machines. In section 4, the comprehensive performances of the two rotor structures are regularly presented. In section 5, the conclusion summarizes what the results obtained and the future work in the next research.

2. ANALYTICAL PROCESS DESIGN

This section presents the inner and outer rotor SPMSMs' analytical designs. The electromagnetic torque (T) is defined via the electromagnetic power (P_e) as in (1) [18].

$$T = \frac{P_e}{2\pi f_1/p} \tag{1}$$

Where p is the number of pole pairs and f_1 is the frequency. According to [18], the shear stress (σ) at the air gap per air unit is as (2).

$$\sigma = \frac{0.5T}{\frac{\pi}{4}D_i^2 L_r} = \frac{\sigma_m}{k_{safe}}, \tag{2}$$

Where k_{safe} is the safe factor, σ_m is the shear stress value and D_i is the rotor's inner diameter. The shaping factor (k_{shape}) of the machine is defined via (3).

$$k_{shape} = \frac{D_i}{L_r} \tag{3}$$

The remanent flux density of PM (B_r) is calculated as (4) [18].

$$B_r = B_{r,o}.\left(1 - T_k.(T_r - T_o)\right) \tag{4}$$

Where T_r is the PM's operating temperature (T_o=30°C), T_k is the temperature coefficient (T_k=0.001), and $B_{r,0}$ is the PM's residual flux density at the environment temperature (T_o=20°C). The flux density in the air gap is defined as (5).

$$B_g = 4.B_m.\frac{\sin(\alpha)}{\pi} \tag{5}$$

Where α is the electrical angle of PM and B_m is the flux density of PM at the working point. Then, the thickness of PM is defined as (6) [19], [20].

$$d_m = \frac{\mu_r\frac{\tau_s}{\tau_s-\gamma g}.g}{\frac{B_r.4\sin(\alpha)}{B_g\pi}-1}, \tau_s = \frac{\pi(D_i-2g)}{Q}, D_i = \left(\frac{4.V_r}{\pi.k_{shape}}\right)^{\frac{1}{3}}, V_r = \frac{0.5T.k_{safe}}{\sigma_m} (6\text{ a}-\text{b}-\text{c}-\text{d}) \tag{6}$$

Where g is air gap thickness, V_r is the rotor volume. From that, the flux of PM can be computed [19]-[21] as (7).

$$\phi_m = B_m.L_r.w_m, \text{for } w_m = \frac{\alpha.D_i}{p} \tag{7}$$

Where w_m is the width of PM. The thickness of the stator yoke (h_{sy}) and rotor yoke (h_{ry}) are determined as (8).

$$h_{sy} = \frac{B_m.w_m}{2B_{sy}}, h_{ry} = \frac{B_m.w_m}{2B_{ry}} \tag{8}$$

Where B_{ry} and B_{sy} are respectively the flux density of rotor and stator yokes. The number of turns for each ended coil is then defined as (9).

$$N = \frac{1.1U_p}{2\sqrt{2}.f.q.k_w.B_{g,pk}.D_i.L_r}, B_{g,pk} = B_g.cos(\delta) \tag{9}$$

Where $B_{g,pk}$ is the maximum flux density, k_w is the winding factor (for concentrated winding, k_w is provided in [21]), U_p is the phase voltage, q is the slot number per phase per pole and δ is the torque angle of the proposed machine ($\delta = 15^0 \div 30^0$). The winding area in each slot is defined as (10).

$$A_w = S_d.N.n_1.2. \tag{10}$$

Where n_1 is the number of conducting bars and S_d is the wire section of one conducting bar. The result for the slot section is now presented in (11) [22], [23].

$$A_{slot} = \frac{A_w}{k_{fill}} \tag{11}$$

Where k_{fill} is the slot-filling factor ($k_{fill} = 0.55$ [21]). The flux on the stator tooth (ϕ_t) and width of the tooth are respectively determined as (12) [24], [25].

$$\phi_t = \frac{\phi_m.2\text{p}}{Q}, w_t = \frac{\phi_t}{L_r.B_t} \tag{12}$$

Where B_t is the flux density on the stator tooth. The bottom width of the stator slot (b_1) and the top width of the stator slot (b_2) are now defined for both inner and outer rotor configurations as in (13), that is,

$$b_1 = \frac{\pi(D_i \pm 2(h_w + h_{so})}{Q} - w_t, b_2 = \sqrt{\frac{{b_1}^2 - 4\,\pi.A_{slot}}{Q}} \quad (13)$$

where h_0 is the height of teeth and h_w is the height of the chork. It should be noted that the sign "+" corresponds to the inner rotor and "+" for the outer rotor. In the end, the stator slot height (h_s) and outer diameter (D_{or}) are determined as (14).

$$h_s = \frac{2A_{slot}}{b_1 + b_2}, D_{or} = D_i \pm 2h_{yr} \quad (14)$$

Where the outer rotor is denoted by the sign "+" and the inner rotor by the sign "+". The (15) can also be used to define the shaft diameter.

$$D_{shaft} = D_o - 2\left(h_{so} + h_w + h_s + h_{sy}\right) \quad (15)$$

Now that the analytical formulas above have been developed, a 7.5 kW practical SPMSM with both inner and outer rotor configurations has been constructed. Table 1 lists the specifications that two of these machines must meet. Table 2 displays the analytical results of the suggested machine for the inner and outer rotors. The FEM in section 3 will confirm these findings. Figures 1(a) and 1(b) show the winding schemes for the inner and outer rotor SPMSMs, respectively.

Table 1. Required parameters of SPMSM with inner and outer rotor configurations

Parameters	Notations	Outer rotor	Inner rotor
Rated power	P_{rated} (kW)	7.5	7.5
Rated voltage	U_{rated} (V)	380	380
Efficiency	η (%)	93	93
Phase number	m	3	3
Frequency	f (Hz)	50	50
Pole number	2p (pole)	12	12
Power factor	cosφ	0.9	0.9

Table 2. Analytical results of SPMSM with inner and outer rotor configurations

Main dimensions	Inner rotor	Outer rotor	Unit
Outer diameter of stator (D_{os})	250	184	mm
Inner diameter of stator (D_{is})	192	102	mm
Outer diameter of rotor (D_{or})	185	221	mm
Shaft rotor diameter	154	192	mm
Rotor length (L_r)	192	192	mm
Stator slot (Q)	12	12	slot
Air gap (g)	1	1	mm
Thickness of PM (d_m)	2.5	2.5	mm

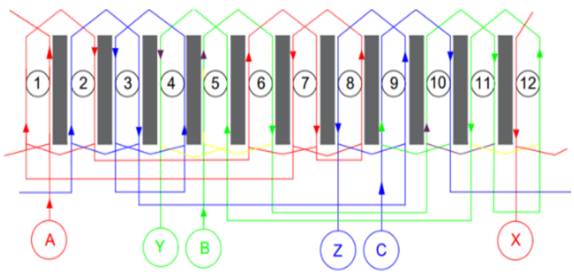

(a)

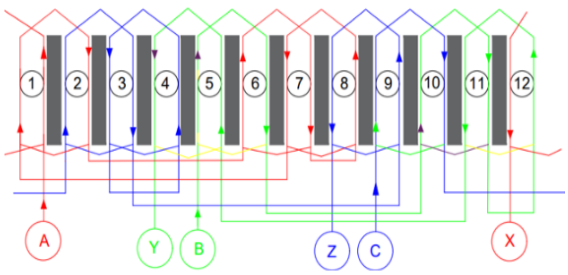

(b)

Figure 1. SPMSM of (a) winding layout of the inner rotor and (b) outer rotor

3. FINITE ELEMENT METHOD

As was mentioned in the preceding section, the analytical model made it easy to calculate differences in design parameters. However, this paradigm only permits defined primary sizes or parameters. Consequently, this section introduces a FEM. In Euclidean space R^3, the set of Maxwell's equations is expressed as (16) [9], [18]:

$$\nabla \times \mathrm{H} = \mathrm{J}_s, \nabla \times \mathrm{E} = -j\omega\, \mathrm{B}, \nabla \cdot \mathrm{B} = 0 \quad (16)$$

where J_s is the current density (A/m^2), H is the magnetic field (A/m), E is the electric field (V/m) and B is magnetic flux density (T). The (16) are solved with constitutive laws and boundary conditions (BCs), as in (17) and (18) i.e., [9].

$$B = \mu H, J = \sigma E \tag{17}$$

$$n \times H|_{\Gamma_h} = 0,\ n \cdot B|_{\Gamma_e} = 0 \tag{18}$$

Where n is the unit normal external to Ω (with $\Omega = \Omega_c \cup \Omega_C^c$), J is the eddy current density (A/m^2), and μ and σ are the relative permeability and electric conductivity (S/m), respectively. It should be noted that the field B in (16) is derived from a vector potential A in (19).

$$B = \nabla \times A. \tag{19}$$

Combining the (16) and (19), the field E is defined via an electric scalar potential φ in (20), that is:

$$E = -\partial_t A - \nabla \cdot \varphi. \tag{20}$$

The electromagnetic field equation written in the Ω (domain of a PM machine) can be represented as [9], [14]–[18]. Based on from (16) to (20), one gets:

$$\nabla \times \left[\frac{1}{\mu}(\nabla \times A - B)\right] + \sigma\, \partial_t A = J_s - \sigma \nabla \cdot \varphi. \tag{21}$$

The linkage flux (ϕ) is then defined as (22).

$$\phi = \frac{L}{S}\left(\iint_{\Omega^+} A d\Omega - \iint_{\Omega^-} A d\Omega\right) \tag{22}$$

Where S is the cross-section area of the conductor length (L). It is simple to determine the back EMF using the linkage flow as given by (22) [18].

4. NUMERICAL RESULTS

Based on the required dimensions obtained from the analytical model given in Table 2, the FEM developed in section 3 is applied to calculate and simulate the magnetic field density, output torque, cogging torque, back EMF, harmonic components of back EMF, flux linkage and temperature rise as well. The comparison of these electromagnetic parameters will be also performed for both inner and outer rotor configurations. Figures 2 and 3 show the 3D modeling of the SPMSM with inner and outer rotor types. The flux density distribution of the two types of SPMSMs is displayed in Figures 4(a) and 4(b). The maximum flux density for the inner rotor SPMSM is 2.134 T, whereas the outer rotor SPMSM has a maximum flux density of 2.442 T. The tooth width and actual slot size are the same for both types of motors. As a result, the SPMSM with an outer rotor type will have a deeper slot than the SPMSM with an inner rotor design. This indicates that the outer rotor SPMSM's teeth will have a higher flux density than the inner rotor SPMSM's. Figure 5 shows the output torque of the SPMSM with the inner and outer rotor designs.

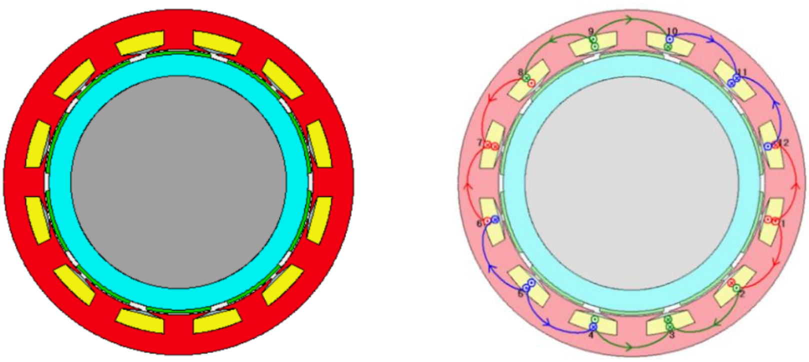

Figure 2. 3D-modelling of SPMSM with inner rotor configuration

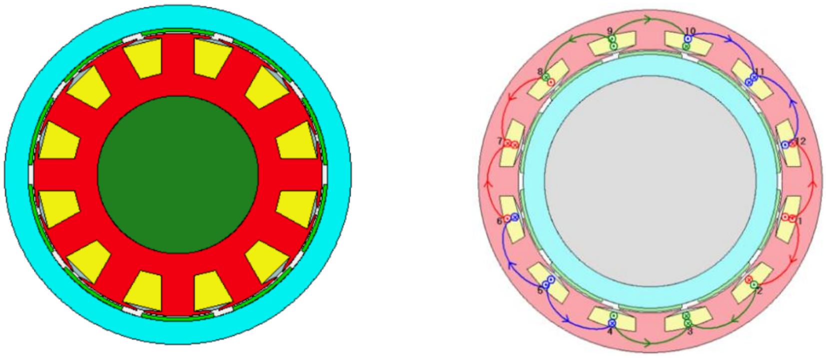

Figure 3. 3D-modelling of SPMSM with outer rotor configuration

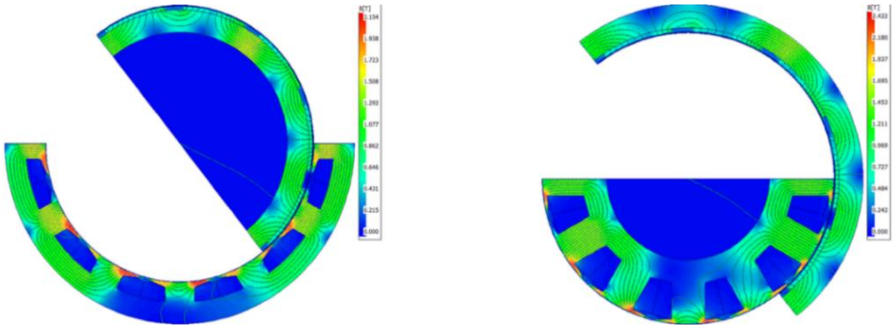

(a) (b)

Figure 4. Configuration of (a) flux density distribution of inner rotor and (b) outer rotor

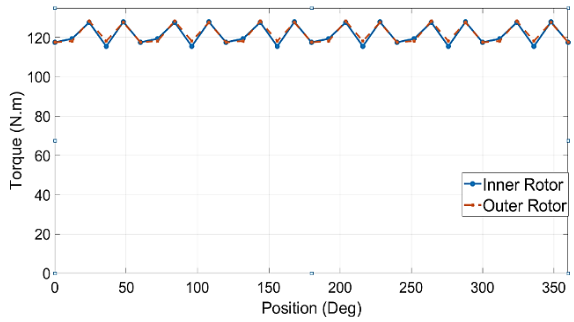

Figure 5. Output torque of inner and outer rotor configurations

The maximum torque of these two motors, 130.812 Nm for the inner rotor SPMSM and 130.824 Nm for the outer rotor SPMSM can be seen to be roughly comparable. In contrast to the inner rotor SPMSM, the outside rotor SPMSM shows a little greater torque. This is explained by the increased torque that is produced by the bigger rotor size in the outer rotor SPMSM. The cogging torque distribution of the SPMSM with inner and outer rotor configurations is shown in Figure 6. The findings show that the inner rotor SPMSM's average cogging torque is 26.814 Nm, while the outer rotor configuration's is 23.953 Nm. This means that the inner rotor SPMSM's average cogging torque is somewhat greater than the outer rotor SPMSM's by 2.888 Nm. This indicates that the cogging torque is lower in the SPMSM with outer rotor construction because its teeth are less than those of the inner rotor type. Consequently, compared to the inner rotor SPMSM, the outer rotor SPMSM will be more stable.

Figure 7 shows the back EMF of the inner and outer rotor designs. Their extremely smooth and sine-shaped waves are seen. In comparison to the inner rotor type, the outside rotor motor's EMF value has a slightly smaller peak. Figure 8 illustrates the torque ripple of the inner and outer rotor designs. The outcome demonstrates that the outer rotor SPMSM's torque ripple is greater than the inner rotor SPMSM's. Uneven torque may result from the outer rotor's size and form interfering with the stator's desired interactions. Figure 9 shows the flux linkage of the inner and outer rotor designs. It should be mentioned that the mean value and waveform of the two machines are rather comparable. The main characteristics of the inner and outer rotor SPMSMs are shown in Table 3. With an efficiency of 94.451%, the inner rotor SPMSM is only 0.195% more efficient than the outer rotor SPMSM, which has a 93.292% efficiency.

As a result, the inner rotor design SPMSM will have losses that are roughly 8 W lower than those of the outer rotor motor. Conversely, the heat dissipation of the inner rotor SPMSM may not be as difficult for the winding coils on the stator as it is for the outer rotor SPMSM. The volumes of these two types of motors are likewise different; the inner rotor SPMSM has a volume that is roughly 0.03 m3 greater than the outer rotor SPMSM. As can be seen, the outer rotor SPMSM has a larger rotor and will produce more torque as a result. This makes it appropriate for applications that need more power, including tractors and cranes. Conversely, the inner rotor SPMSM's smaller rotor offers faster speeds and is frequently used in applications where compactness is crucial, like electric automobiles and motorbikes. These machines' temperature issue is also looked into. Figures 10 through 13 show the thermal circuit map and arrangement for the outer and inner rotor designs. Table 4 shows the temperature rise value at the various positions of the inner and outer rotor SPMSMs.

With an average temperature differential of 14.87 °C, it is evident that the outer rotor's temperature is higher than the inner rotor's in every position. To be more precise, the stator slot has the largest temperature difference (24.4 °C) and the rotor slot has the lowest (1.1 °C). This is due to the fact that heat dissipation is more difficult for the outer rotor as the winding experiences the greatest heat loss. The winding is located inside the stator. To facilitate heat dissipation, the inner rotor's winding is wrapped around an external stator. Heat dissipation is further complicated by the air gap between the rotor slots in the outer rotor SPMSM. As a result, the outer rotor motor's temperature rise is greater than the inner rotor motors.

Table 3. FEM results

Parameters	Inner rotor	Outer rotor	Unit
Efficiency	93.930	93.568	%
Output torque	119.66	119.73	Nm
Torque ripple	9.7452	8.0953	%
Power factor	0.9572	0.9406	
Output power	7518.7	7522.7	W
Total losses	502.98	517.12	W
Volume	0.00942	0.00737	m^3

Table 4. Temperature rise

Position	Inner rotor (°C)	Outer rotor (°C)
Shaft	67.3	91.2
Teeth	67.5	91.4
Slot	76.5	96
Rotor yoke	67.4	65.8
Stator yoke	67.3	91.8
Permanent magnet	67.4	66.4

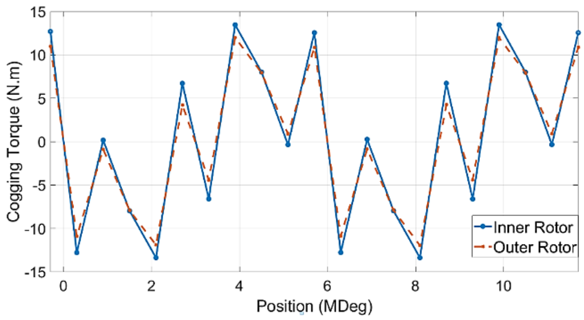

Figure 6. Cogging torque of inner and outer rotor configurations

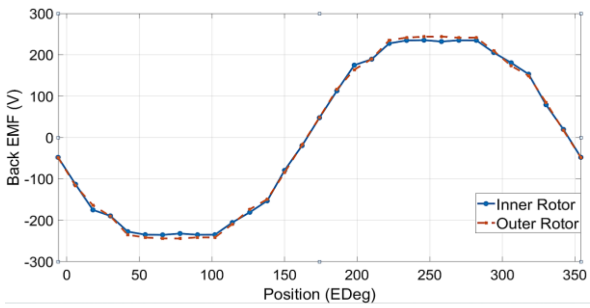

Figure 7. Back EMF of inner and outer rotor configurations

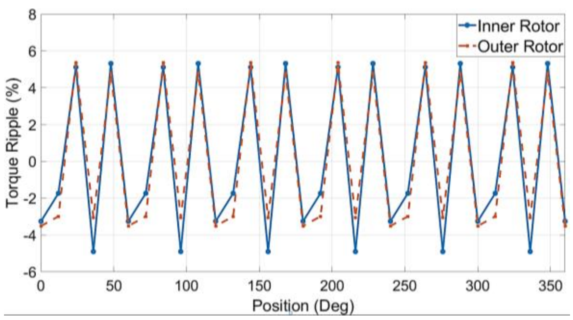

Figure 8. Torque ripple of inner and outer rotor configurations

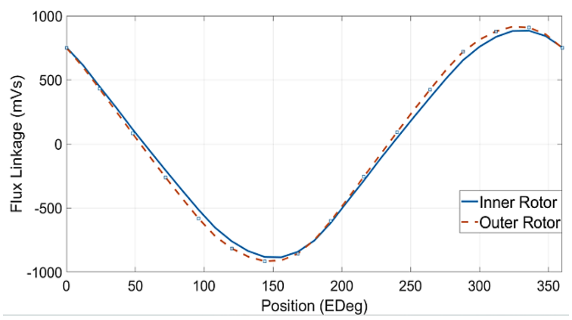

Figure 9. Flux linkage of inner and outer rotor configurations

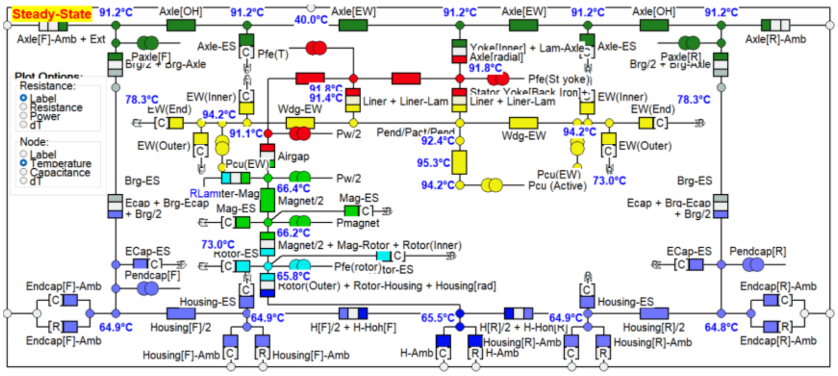

Figure 10. Layout of the thermal circuit of the outer rotor

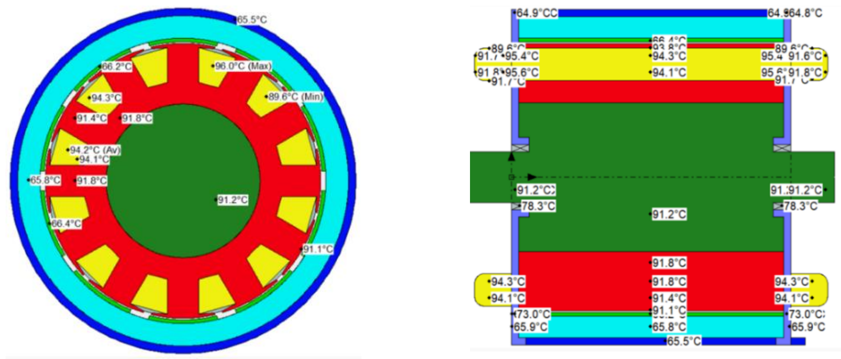

Figure 11. Temperature rise of outer rotor configuration

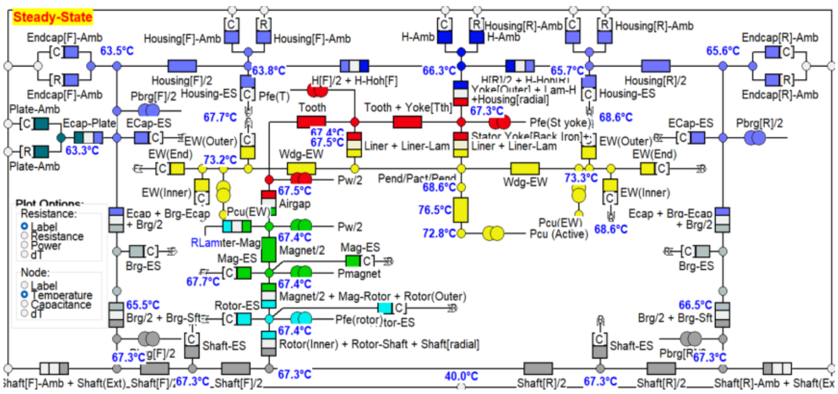

Figure 12. Layout of the thermal circuit of the inner rotor

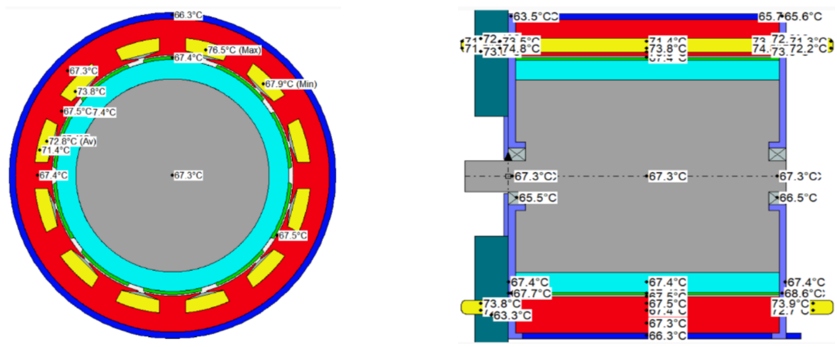

Figure 13. Temperature rise of inner rotor configuration

5. CONCLUSION

In this context, the combination of the analytical design and FEM 5 have been successfully developed for the SPMSMs with inner and outer rotor configurations. The results on electromagnetic parameters such as the flux density, back EMF, output torque, cogging torque, torque ripple, flux linkage, and temperature rise of the proposed SPMSM were obtained. In particular, via the FEM, the paper has concentrated on the comparative design of the inner and outer rotor SPMSMs with concentrated winding to identify their advantages and disadvantages of each motor. using the analytical approach and FEM. The acquired data showed that both inner and outer rotor SPMSM types operate well but with different advantages and disadvantages. Compared to the outer rotor SPMSM, the inner rotor SPMSM has the advantages of higher speed and lower temperature. In contrast, the outer rotor SPMSM outperforms the inner rotor SPMSM in terms of torque and stability. This work also serves as a foundation for further research, including possible directions such as optimizing design computations using optimization methods like swarm optimization and evolutionary algorithms, among others. In addition, based on the performances obtained from each machine, will provide a valuable reference for choosing the SPMSM with inner or outer rotor structure for traction applications. However, the results obtained from the proposed methods are very reliable and acceptable. However, an experiment model has not been performed yet in this study. It will be done in the next research to validate perfectly the development of the methods.

REFERENCES

[1] Z. Wang, J. Gong, and B. Liu, “Multi-objective optimization of the hollow shaft direct drive motor,” *Advances in Mechanical Engineering*, vol. 15, no. 3, p. 168781322311630, Mar. 2023, doi: 10.1177/16878132231163079.

[2] M. Wang, L. Wang, R. Huang, and C. Yang, “Event-based disturbance compensation control for discrete-time SPMSM with mismatched disturbances,” *International Journal of Systems Science*, vol. 52, no. 4, pp. 785–804, Mar. 2021, doi: 10.1080/00207721.2020.1840650.

[3] Peng Zhang, G. Y. Sizov, and N. A. O. Demerdash, “Comparison of torque ripple minimization control techniques in Surface-Mounted Permanent Magnet Synchronous Machines,” in *2011 IEEE International Electric Machines & Drives Conference (IEMDC)*, May 2011, pp. 188–193, doi: 10.1109/IEMDC.2011.5994641.

[4] L. Feng, S. Yu, F. Zhang, S. Jin, and Y. Sun, “Study on performance of low-speed high-torque permanent magnet synchronous motor with dynamic eccentricity rotor,” *Energy Reports*, vol. 8, pp. 1421–1428, Aug. 2022, doi: 10.1016/j.egyr.2022.03.018.

[5] E. El-Kharashi, “Approaches to prove the rotor of the permanent magnet machine must be outside in order to improve the energy conversion process,” *International Journal of Applied Electromagnetics and Mechanics*, vol. 47, no. 1, pp. 141–152, Jan. 2015, doi: 10.3233/JAE-140003.

[6] L. I. Jusoh, E. Sulaiman, F. S. Bahrim, and R. Kumar, “Design Comparison of Inner and Outer Rotor of Permanent Magnet Flux Switching Machine for Electric Bicycle Application,” in *IOP Conference Series: Materials Science and Engineering*, Aug. 2017, vol. 226, p. 012129, doi: 10.1088/1757-899X/226/1/012129.

[7] S. J. Kim, E. J. Park, S. Y. Jung, and Y. J. Kim, “Transfer Torque Performance Comparison in Coaxial Magnetic Gears with Different Flux-Modulator Shapes,” *IEEE Transactions on Magnetics*, vol. 53, no. 6, 2017, doi: 10.1109/TMAG.2017.2663429.

[8] W.-S. Jung, H.-K. Lee, Y.-K. Lee, S.-M. Kim, J.-I. Lee, and J.-Y. Choi, “Analysis and Comparison of Permanent Magnet Synchronous Motors According to Rotor Type under the Same Design Specifications,” *Energies*, vol. 16, no. 3, p. 1306, Jan. 2023, doi: 10.3390/en16031306.

[9] J.-Y. Choi, H.-I. Park, S.-M. Jang, and S.-H. Lee, “Design and Analysis of Surface-Mounted PM Motor of Compressor for Electric Vehicles Applications according to Slot/Pole Combinations,” *The Transactions of The Korean Institute of Electrical Engineers*, vol. 60, no. 10, pp. 1846–1857, Oct. 2011, doi: 10.5370/KIEE.2011.60.10.1846.

[10] H. Murakami, Y. Honda, H. Kiriyama, S. Morimoto, and Y. Takeda, “The performance comparison of SPMSM, IPMSM and SynRM in use as air-conditioning compressor,” in *Conference Record of the 1999 IEEE Industry Applications Conference. Thirty-Forth IAS Annual Meeting (Cat. No.99CH36370)*, vol. 2, pp. 840–845, doi: 10.1109/IAS.1999.801607.

[11] S.-K. Cho, K.-H. Jung, and J.-Y. Choi, “Design Optimization of Interior Permanent Magnet Synchronous Motor for Electric Compressors of Air-Conditioning Systems Mounted on EVs and HEVs,” *IEEE Transactions on Magnetics*, vol. 54, no. 11, pp. 1–5, Nov. 2018, doi: 10.1109/TMAG.2018.2849078.

[12] Z. Q. Zhu and D. Howe, “Influence of design parameters on cogging torque in permanent magnet machines,” *IEEE Transactions on Energy Conversion*, vol. 15, no. 4, pp. 407–412, 2000, doi: 10.1109/60.900501.

[13] G. Du, N. Li, Q. Zhou, W. Gao, L. Wang, and T. Pu, “Multi-Physics Comparison of Surface-Mounted and Interior Permanent Magnet Synchronous Motor for High-Speed Applications,” *Machines*, vol. 10, no. 8, p. 700, Aug. 2022, doi: 10.3390/machines10080700.

[14] Y. Xia, J. Li, R. Qu, and H. Fang, “Comparison of two rotor topologies for high-speed permanent magnet synchronous machines,” in *2016 XXII International Conference on Electrical Machines (ICEM)*, Sep. 2016, pp. 1419–1425, doi: 10.1109/ICELMACH.2016.7732710.

[15] X. Liu, Z. Zhang, J. Xiao, and H. Xu, “Comparison and analysis of electromagnetic characteristics of IPMSM with single and double layer PMs,” *International Journal of Applied Electromagnetics and Mechanics*, vol. 58, no. 4, pp. 483–496, Dec. 2018, doi: 10.3233/JAE-180032.

[16] J. Dong, Y. Huang, L. Jin, and H. Lin, “Comparative Study of Surface-Mounted and Interior Permanent-Magnet Motors for High-Speed Applications,” *IEEE Transactions on Applied Superconductivity*, vol. 26, no. 4, pp. 1–4, Jun. 2016, doi: 10.1109/TASC.2016.2514342.

[17] M. Arehpanahi and E. Kheiry, “A new optimization of segmented interior permanent magnet synchronous motor based on increasing flux weakening range and output torque,” *International Journal of Engineering Transactions C: Aspects*, vol. 33, no. 6, pp. 1122–1127, Jun. 2020, doi: 10.5829/ije.2020.33.06c.09.

[18] V. X. Hùng, “Modeling of Exterior Rotor Permanent Magnet Machines With Concentrated Windings,” Universiteit Delft, 2018. [Online] Available: https://repository.tudelft.nl/record/uuid:27bb59c4-14c8-45fe-9284-28363b46e060.

[19] M. Ojaghi, M. Sabouria, J. Faizb, and V. Ghorbanianb, “Exact modeling and simulation of saturated induction motors with broken rotor bars fault using winding function approach,” *International Journal of Engineering, Transactions A: Basics*, vol. 27, no. 1, pp. 69–78, 2014, doi: 10.5829/idosi.ije.2014.27.01a.10.

[20] T. Pu, G. Du, J. Tong, N. Huang, N. Li, and W. Xu, “Comparison of Rotor Strength of Various Rotor Structures for Ultra-high-speed Permanent Magnet Synchronous Motor,” in *2021 IEEE 4th Student Conference on Electric Machines and Systems (SCEMS)*, Dec. 2021, pp. 1–6, doi: 10.1109/SCEMS52239.2021.9646110.

[21] M. Sahebjam, M. B. Bannae Sharifian, M. R. Feyzi, and M. Sabahi, "Novel unified control method of induction and permanent magnet synchronous motors," *International Journal of Engineering, Transactions B: Applications*, vol. 32, no. 2, pp. 284–291, 2019, doi: 10.5829/ije.2019.32.02b.11.

[22] D. G. Dorrell, M.-F. Hsieh, M. Popescu, L. Evans, D. A. Staton, and V. Grout, "A Review of the Design Issues and Techniques for Radial-Flux Brushless Surface and Internal Rare-Earth Permanent-Magnet Motors," *IEEE Transactions on Industrial Electronics*, vol. 58, no. 9, pp. 3741–3757, Sep. 2011, doi: 10.1109/TIE.2010.2089940.

[23] D. Martínez, "Design of a Permanent-Magnet Synchronous Machine with Non- Overlapping Concentrated Windings Design of a Permanent-Magnet Synchronous Machine with Non-Overlapping Concentrated Windings for the Shell Eco Marathon Urban Prototype," pp. 66–114, 2012.

[24] T. C. Truong, T. N. Vu, H. B. Duc, and V. D. Quoc, "Using Genetic Algorithms for Optimal Electromagnetic Parameters of SPM Synchronous Motors," *Journal Europeen des Systemes Automatises*, vol. 56, no. 6, pp. 899–906, 2023, doi: 10.18280/jesa.560601.

[25] J. M. Crider and S. D. Sudhoff, "An Inner Rotor Flux-Modulated Permanent Magnet Synchronous Machine for Low-Speed High-Torque Applications," *IEEE Transactions on Energy Conversion*, vol. 30, no. 3, pp. 1247–1254, 2015, doi: 10.1109/TEC.2015.2412547.

BIOGRAPHIES OF AUTHORS

Hoang Bui Huu received an engineering degree in 2023 from the School of Electrical and Electronic Engineering, Hanoi University of Science and Technology. He is currently working as a master's student at Hanoi University of Science and Technology. He can be contacted at email: hoang.bh241170M@sis.hust.edu.vn.

Bao Doan Thanh received a B.S. degree in Electrical engineering from Hanoi University of Science and Technology, Vietnam in 2006, an M.S. degree from Hanoi University of Science and Technology, Vietnam, in 2010, and the Ph.D. degree from Hanoi University of Science and Technology, in 2016. He is currently working as a lecturer at the Faculty of Engineering and Technology, Quy Nhon University, Vietnam. His research interests include electrical power systems, switching devices, electrical machines and transformers; calculation of magnetic fields and electromagnetic. He can be contacted at email: doanthanhbao@qnu.edu.vn.

Tran Duc Chuyen received a Ph.D. degree in Industrial Automation from Le Qui Don Technical University (MTA), Hanoi, Vietnam in 2016. Now, he works at the Faculty of Electrical Engineering - Automation, University of Economics-Technology for Industries. He is currently the president of the Council of the Science of the Faculty of Electrical Engineering. Dr Tran Duc Chuyen′s main research: electric machines, drive systems, control theory, power electronics and applications, adaptive control, neural network control, automatic robot control, motion control, IoT, intelligent control, and artificial intelligence. He can be contacted at email: tdchuyen@uneti.edu.vn.

Vuong Dang Quoc received his Ph.D. degree in 2013 from the Faculty of Applied Sciences at the University of Liège in Belgium. After that, he came back to the Hanoi University of Science and Technology in September 2013, where he is currently working as a deputy director of the Training Center of Electrical Engineering, School of Electrical Engineering, Hanoi, University of Science and Technology. He became an associate professor in 2020. Assoc. Prof. Dang Quoc Vuong's research domain encompasses the modeling of electromagnetic systems, electrical machines, optimization methods, numerical methods, and subproblem methods. He can be contacted at email: vuong.dangquoc@hust.edu.vn.